Asociación Argentina
de Mecánica Computacional

Mecánica Computacional Vol XXXIX, págs. 397-406 (artículo completo)
F.E. Dotti, M. Febbo, S.P. Machado, M. Saravia, M.A. Storti (Eds.)
Bahía Blanca, 1-4 Noviembre 2022

SCALE ADAPTIVE SIMULATIONS APPLIED TO FULLY CAVITATING TURBULENT FLOW IN INJECTOR NOZZLES

Miguel G. Coussirat[a], Tomás Leschiutta[b], Flavio H. Moll[a]

[a]Grupo UTN LAMA- Universidad Tecnológica Nacional - Facultad Regional Mendoza, Argentina, miguel.coussirat@frm.utn.edu.ar, http://www.frm.utn.edu.ar
[b]Centro de Investigación de Métodos Computacionales (CIMEC),CONICET/UNL, Predio CONICET Santa Fe - Colectora Ruta Nac Nro 168, Paraje El Pozo, Santa Fe, Argentina, http://www.cimec.org.ar

Keywords: Developed Cavitation, Injectors, Turbulence, Eddy Viscosity Models, SAS Validation/Calibration.

Abstract: The unsteady and turbulent pressure-driven cavitating flow under fully cavitation conditions through a sharp-edged orifice is studied by numerical simulations. Unsteady cavitating flow is a typical flow configuration in fuels injectors and brings a challenge in the numerical modeling of two-phase fluid flows due to the high-pressure gradients involved and the high ratio of liquid and vapor density. Under this flow condition computationally intensive unsteady simulations are necessary to accurately simulate the irregular cyclic process of bubble formation, growth, filling by water jet re-entry and its breakoff. The capabilities of Reynolds Averaged Simulations are assessed to ensure a suitable cavity structure prediction to capture the main shedding frequencies and the vapor fraction variations along the nozzle. This study is focused on the performance of a modified version of the Shear Stress Transport turbulence model, involving a Scale Adaptive Simulations sub-model related to the unsteady turbulent flows modeling. The obtained results show that the proposed option would allow studies of developed cavitating flows by means of an unsteady Reynolds Averaged Simulation, computationally less expensive than the Large Eddy Simulations option, being this last option not completely affordable for simulating turbulent flows in industrial problems nowadays.

1. INTRODUCTION

In liquid flows, cavitation occurs if the local pressure p_c drops below the vapor pressure p_v in certain locations. This local low-pressure level provokes that the initial liquid flow becomes a two-phase flow, i.e., liquid-bubbles of gas/vapor. The presence of undissolved gas particles, boundary layers, and turbulence will modify this surface stress and often mask a departure of this critical pressure p_c from p_v, Coussirat et al., 2016. Cavitation always involves complex interactions between turbulent flow structures and multiphase dynamics in internal and external flows, Singhal et al., 2002, Korkut et al., 2002, Sou et al, 2014. The viscous nature of the flow, particularly the interaction between the free-stream turbulence and the boundary layer is one of the main factors contributing to the scale effects on the inception of cavitation. A high turbulence level causes early laminar/turbulent transition in the boundary layer, which, in turn, can lead to the elimination of the laminar separation having a major effect on the cavitation inception.
Because studies by physical experiments are very expensive (high-speed flow and small spatial- and time- scales involved), Computational Fluid Dynamics (CFD) codes, based on a certain kind of 'multiphase flow modeling technique' have been specifically adapted/developed for studying cavitating flows entailing both the turbulence and the mass transfer modeling. Thus, a steady or unsteady Reynolds Averaged Simulations (RAS/URAS) plus Eddy Viscosity models (EVMs) for the incompressible mixture (liquid+vapor) joined to a model for computing the vapor fraction of the mixture (*vf*), using a Transport Equation-based Modeling (TEM) technique for the cavitating flow modeling, constitutes the complete model, (i.e., RAS/URAS+EVMs+TEM technique). In fuel injectors for Diesel engines, the occurrence of cavitation inside an injector nozzle plays a significant role in the spray atomization at its outlet, see Fig.1.

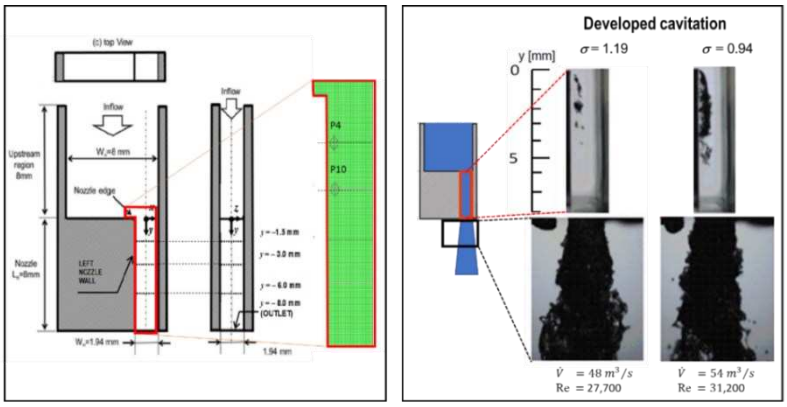

Fig.1. Geometry, zoom of the mesh M03 in the step zone (in red) and experimental data , Sou et al., 2014
Notation: P4 and P10: positions for CFD frequency analysis.

The type of atomization induced by cavitation allows developing efficient devices when this cavitation state is controlled. The obtained results by RAS in cases of incipient cavitation showed a higher dependence on the EVMs than on the TEMs selected. A careful EVM calibration allows to capture several of the incipient cavitating flow characteristics due to the close relation between the cavitation state and the turbulence level in the flow. This is related to the spatial distribution of the computed mixture eddy viscosity level, $\nu_{t,m}$, defined by a suitable turbulence scaling that depends on the EVM used. Under the cavitation process some preferred turbulence scales appear leading to a 'non-standard turbulence state' as experiments show. So, cavitating flows should not be modeled as simple shear flow. Under incipient cavitation in nozzles, uncalibrated EVMs overpredict the $\nu_{t,m}$ level and therefore, lower dynamic pressure levels are computed yielding a higher static pressure and less *vf*. This fact directly affects the cavity shape due to the high stresses computed, keeping down the velocity predictions in the recirculation zones, Shi et al., 2010, Biçer

2015, Coussirat et al., 2016. When the flow into the nozzle falls under fully developed cavitation state, an unsteady shedding flow pattern appears in the flow affecting the local pressure levels in the nozzle. Uncalibrated EVMs do not capture this shedding pattern in a suitable way, Coussirat et al., 2021a,b. Then, URAS simulations based on the 'classic' EVMs predict a limited range of unsteady flow features and are not optimal for the simulation of the turbulent structures in highly separated flows. URAS models need special treatment at the cut-off limit allowing the formation of a turbulent spectrum. As such models are based on transport equations (TEQs) with no information on the grid spacing, they will attempt to transfer the energy through the entire cascade down to the Kolmogorov limit i.e., to the dissipative turbulence scales. However, like in Large Eddy Simulations (LES), this is not possible because the 'affordable' resolution is not sufficient for this transfer, Egorov et al., 2008, Thing 2016. Therefore, some information on the grid spacing and a suitable time-step will have to be supplied to such methods. In principle, this must be true for all URAS-like methods with scale-resolving capability.

The goal of this work is to explore URAS models that incorporates the Scale Adaptative Simulation technique (SAS), Egorov et al., 2008, Egorov et al., 2010, Menter et al., 2010, where no explicit grid dependency is introduced into the equations unlike LES or Detached Eddy Simulations (DES). In previous works from Coussirat et al., 2021a,b the Shear Stress Transport k-ω (SST) model from Menter, 1994 showed good predictive capabilities in RAS simulations of incipient cavitating flows in nozzles and now, the performance of optimized SST by SAS (SAS-SST) is studied in deep. The obtained results show that it resolves some features of the unsteady flow accounting for the influence of turbulence structures on the spray formed at the injector outlet, without the high computing requirements needed for standard DES/LES simulations. To avoid the high CPU cost associated with DES or LES simulations, the URAS+SAS-SST simulation is assessed when it is applied to nozzles working under fully developed cavitation conditions. The obtained results show the possibility to go further away from equilibrium and to account for the streamline curvature effects (e.g., vortices/eddies) but without any explicit grid-dependence of the solution as DES or LES simulations need.

2. METHODOLOGY DEVELOPED FOR URAS/SAS MODELING

Developed cavitating flows are studied by URAS simulations in a low-pressure Diesel injector with an asymmetrical nozzle inlet configuration and square sections at the outlet using the SST and the SAS-SST model coupled with the TEM model from Singhal et al., 2002. Ad-hoc calibration strategies for the used EVMs are again applied because it was demonstrated the significance in to pay more attention in a detailed EVMs calibration than in the TEMs ones in cases of incipient cavitating flow, Coussirat et al., 2016-2021a,b. The experiments from Sou et al, 2014 are used for the cavity shape comparisons and EVMs calibrations, see Fig.1. Complementary experimental results related to the eddies shedding frequencies in cavitating flows from De Giorgi et al 2013, Stanley et al., 2014, Biçer 2015, Gavaises et al., 2015, Zixhia et al., 2016, Wang et al., 2018 and Trummler et al., 2020 are also used for the validation/calibration tasks.

2.1. EVMs used: the SST k-ω (SST) and the SAS SST k-ω (SAS-SST) models.

The EVMs selected were the SST and the SAS-SST, Eqs.1-4. Full details of these two EVMs can be seen in Menter, 1994, Menter et al., 2003, Menter et al., 2005, Versteeg et al., 2007, Egorov et al., 2008, Egorov et al., 2010, Menter et al., 2010. The SST model belongs the so-called 'Two-Equation EVM models', Eqs.1-4, being this model a hybrid model combining the Wilcox Standard k-ω (Sko) and the Launder and Spalding Standard k-ε (Ske) models by using the blending F_1 and F_2 functions. These functions activate the Sko model near the wall and the Ske model in the free stream zones ensuring that the appropriate model is used throughout the flow field. The blending procedure to obtain the TEQs for the SST model leads to the Shear Stress Transport term

definition, i.e., the damped cross-diffusion term, (4th term, right side in the Eq.2), being this term distinctive of the SST model when it is compared against the Sko model. There are some differences in the Eqs.1-4 for the SST and the SAS-SST models, i.e., when the SAS option is selected in the ω-TEQ, Eq.2, the Q_{sas} term appears, Eqs.3,4.

$$\frac{\partial \rho k}{\partial t}+\frac{\partial \rho u_i k}{\partial x_i}=P_k+\frac{\partial}{\partial x_i}\left[\left(\frac{\mu_T}{\sigma_k}+\mu\right)\frac{\partial k}{\partial x_i}\right]-\rho\beta^* f_{\beta^*} k\omega;\ P_k=\mu_T S^2;\ S=\sqrt{2S_{ij}S_{ij}}\,, \tag{1}$$

$$\frac{\partial \rho \omega}{\partial t}+\frac{\partial \rho u_i \omega}{\partial x_i}=\alpha\left(\frac{\omega}{k}\right)P_k+\frac{\partial}{\partial x_i}\left[\left(\frac{\mu_T}{\sigma_\omega}+\mu\right)\frac{\partial \omega}{\partial x_i}\right]-\rho\beta f_\beta \omega^2+(1-F_1)\frac{2\rho}{\omega\,\sigma_{\omega,2}}\frac{\partial k}{\partial x_j}\frac{\partial \omega}{\partial x_j}+Q_{SAS}\,, \tag{2}$$

$$Q_{SAS}=max\left\{P_{SAS}-C_{SAS}f_1\left[\rho k, max\left(\frac{|\nabla\omega|^2}{\omega^2},\frac{|\nabla k|^2}{k^2}\right)\right],0\right\};P_{SAS}=f_2[\rho\varphi_{SAS}\kappa S^2(L/L_{vK})^2], \tag{3}$$

$$\nu_{t,m}=f_3(\rho,k,\omega,F_2);\ L=f_4(k^{1/2}\omega^{-1});\ L_{vK}=\max\left[f_5(S,(|\nabla^2 u|)^{-1});f_6\left(C_s,V_{cell}^{1/3}\right)\right]. \tag{4}$$

In these equations $\sigma_k,\sigma_\omega,\beta^*_\infty,\varphi_{SAS},\kappa,C_{SAS},C_s$ are the calibration constants of the turbulence model; $\alpha,\beta,\beta^*=f(\beta^*_\infty,\mathrm{Re}_\tau),f_{1-5},f_\beta=f(\beta^*_\infty),\ f_{\beta^*}$ are empirical functions, $\mathrm{Re}_\tau=\rho k(\mu\omega)^{-1}$ and V_{cell} is the mesh cell volume. The functions $f_{1\text{-}5}$ point out the dependence among the consigned dependant variable and the independent parameters in each of these functions.

The SAS concept is a technique for adapting the length scales automatically instead of the more expensive LES option in terms of CPU requirements, allowing the resolution of the turbulence spectrum in transient flow conditions. The used version of SAS is coupled to the SST model to recover the SST performance when it is used in boundary layer (BL) flows. The SAS extension was formulated as an extra production term to the ω-TEQ, Eq.2, i.e., the Q_{SAS} term, which does not disturb the SST model behavior for steady BL flows but activates the 'SAS mechanism' when instabilities appear into the flow. This term is sensitive to resolved fluctuations (i.e., unsteadiness), because when the RAS/URAS+EVMs equations compute turbulence the length scale based on velocity gradients is much smaller than that based on time-averaged velocity gradients $\partial U_i/\partial x_j$. In SAS this fact is related to the ad-hoc defined von Kármán length scale, L_{vK}, Eq.4, in addition to the standard input for the length scale based in $\partial U_i/\partial x_j$, constituting an appropriate quantity to use as a sensor for detecting unsteadiness in the model. The L in the P_{SAS} source term Eq.3 is the length scale of the modeled turbulence, i.e., $L=f(k^{0.5}\omega^{-1})$, and the von Karman length scale L_{vK} is a three-dimensional generalisation of the classic boundary layer definition, i.e., $L_{vK}=g[(\partial U/\partial y/(\partial^2 U/\partial y^2)]$. So, the defined L and L_{vK} are both equal to (κy) in the logarithmic part of the BL, being κ the von Karman constant, Egorov et al., 2008. The objective of the Q_{SAS} term is to increase ω in regions where the flow is on the limit of going unsteady. The result is a computed reduction in k and $\nu_{t,m}$ levels, so that the modeled dissipation (i.e., the damping effect) of the $\nu_{t,m}$ on the resolved fluctuations is reduced, thereby promoting the momentum equations to switch from steady to unsteady mode. The Q_{sas} term calibration allows to obtain a reduced $\nu_{t,m}$ level provoking the apparition of cavitation conditions in the simulated cases in nozzles, being similar as one already performed when the constant β^*_∞ was calibrated ad-hoc to modify the ω-production/k-dissipation terms, see Eqs.1,2, Coussirat et al., 2021a. In the Eq.4 the calibration constant C_s provides a similar condition as β^*_∞ but now as a lower limit constraint exerting a direct control over the high wave number damping, i.e., its purpose is to control the finest resolved turbulent fluctuations damping related to the L_{vk} scale. The SAS strategy implies that the resolved turbulence is of the same scale as the grid spacing ($V_{cell}^{1/3}$) at the high wave number limit. In this limit, the energy which is transported down across the turbulent spectrum by vortex stretching and break-up must be dissipated. This situation is like standard LES methods, where the main effect of the subgrid $\nu_{t,m}$ is the energy dissipation from the smallest resolved scales. Since the SAS concept automatically adjusts to the resolved scales (i.e., the smallest scales in the simulation) the model does not require

any special provisions for damping small scales, but could provide an adequate level of $\nu_{t,m}$ without modification, Egorov et al., 2008. The functionality of SAS is like the DES, being it a hybrid formulation that uses both EVMs and LES. The LES activity in LES/DES modeling is enforced by the grid limiter, whereas SAS allows a breakdown of the large unsteady structures by adapting the EVM to the locally resolved length scale, because the SAS provides two independent scales for the source terms of the underlying SST model, Egorov et al., 2010, Menter et al., 2010. This functionality is explored here to open the possibility to perform URAS/EVM CFD obtaining resolved unsteady cavity structures with affordable CPU costs in cases involving complex 3D geometries in the future, due to SAS would allow URAS flow studies including a technique for adapting the length scales automatically instead of the more expensive DES/LES option in terms of CPU requirements.

2.2. Two-phase/cavitating flow: Transport Equation-based Modeling (TEM) models

This technique consists in solving a transport equation for either mass or volume fraction with appropriate source terms to regulate the mass transfer between phases. The TEM from Singhal et al., 2002 was selected, because it showed a good performance in cavitating flow cases for several nozzle geometries, Coussirat et al., 2017-2021a,b. The original calibration of this model was performed under the assumption of isotropic turbulence, despite that in BL flows the turbulence is anisotropic, Singhal et al., 2002. It is remarked that it is necessary to compute previously a suitable $\nu_{t,m}$ level in the cavitation zone for a subsequent appropriate pressure field prediction under slightly or fully developed cavitation conditions. This fact led to a more careful EVMs calibration than in the TEM used, although perhaps the TEM tuning should be revisited more in detail in the future.

2.3. Experimental databases used

Due to the high-speed flow and small spatial and time scales involved, the study of cavitating flows using physical experiments is very hard and expensive, see full details in Coussirat et al., 2016-2021a,b. For URAS/EVM CFD the showed cavitation states shown in Fig.1 are classified by a two characteristic numbers, i.e., Reynolds (Re) and Cavitation (σ) numbers:

$$\sigma = \frac{(p_{out} - p_v)}{0.5\rho c_{m,out}^2};\ \mathrm{Re} = \frac{c_{m,out} w_n}{\nu};\ \mathrm{We} = \frac{\rho c_{m,out}^2 th_n}{\tau_s};\ \mathrm{Sr} = \frac{f_{vs} L_{cav}}{c_{m,out}} \tag{5}$$

Also, the Weber (We) and the Strouhal (Sr) numbers are commonly used for defining related conditions in cavitating flows cases, Coussirat et al., 2017-2021a,b. In Eq.5 w_n, th_n are the nozzle width and thickness respectively; $L_{cav}=f(L_n)$ is the mean cavity length; L_n is the nozzle length; $c_{m,out}$ is the outlet mean velocity; f_{vs} is the eddies shedding frequency; ν is the liquid viscosity ($=1.035\times10^{-6}$m^2/s); ρ is the liquid density ($=998$kg/m^3); τ_s is the liquid surface stress ($=7.28\times10^{2}$N/m); p_{out} is the outlet pressure ($=1.0\times10^{5}$Pa) and p_v is the vapor pressure ($=2{,}300$Pa). The different σ cases were generated by changing the flow rate, because the p_{out} remains constant having a subsonic free jet flow at the outlet with negligible surface stresses due to the We computed was of O(10), despite the small outlet nozzle dimensions.

In nozzles, the Sr characterizes the periodic flow motion and the cavity evolution owing to the inertial forces and the velocity changes related with the convective acceleration of the flow field. When the cavitation migrates from incipient to slightly developed, (i.e., σ=1.19) flow instabilities start to appear, Wang et al., 2018, Stanley et al., 2014, Sou et al, 2014, Biçer 2015.

For a $10^{-4}<$ Sr <1 range the oscillations are characterized by the build-up and rapidly subsequent vortex shedding. The flow shows a clear periodic behavior as the σ increases, being this related to the 're-entrant jet process' that provokes the cavity periodic shedding, a common form of cavitation instability. The Sr values must be treated as nominal, since they have been defined in

terms of an average velocity within the nozzle determined by the imposed flow rate despite the flow velocity at the contraction region could be significantly higher, Mitroglou et al., 2017.
An important parameter to account for this unsteadiness is the eddies/cavity shedding frequency, f_{vs}, related with the Sr number. Experiments from Stanley et al., 2014 reported that in a circular nozzle (D=8.25mm, 6.9×10^4<Re<2.19×10^5) cavitation occupied less than 30% of the nozzle length, exhibiting a periodic bubble cloud shedding, with a fundamental frequency (f_{vs} 1st mode) between 0.5 and 2kHz. Experiments in square section nozzles from Zixhia et al., 2016 report a f_{vs}1st mode of 2,800Hz (w_{th}=2mm, σ=1.008, Re=13,500). Ones from Biçer 2015, see Fig.2, showed a partial cavity evolution for σ=0.94, but there is no information on f_{vs} values. On the other hand, a CFD investigation of the re-entrant jet dynamics in a cavitating nozzle flow by means of LES was performed by Trummler et al., 2020 computing a f_{vs}1st mode of 1,110Hz, and 750 Hz for the Sou et al, 2014 σ=1.19, Re=2.77×10^4 and σ=0.82-0.84, Re=3.35×10^4 cases respectively. Notice that when the orifice area diminishes or the σ rises, the shedding frequency rises, Stanley et al., 2014, Gavaises et al., 2015.
Several attempts were made to identify the *vf* into the cavity. Experiments from Sou et al, 2014 and Biçer 2015 showed some representative images for the 'mean' transient cavity obtained for each cavitation state, see Fig.1, but unfortunately *vf* values were not reported into the cavity. LES/CFD simulations from Trummler et al., 2020 showed that the *vf* computed has strong variations into the cavity for the Sou cases. Moreover, the vortices appear with a subsequent shedding downstream. They are also accompanied by clouds of vapor bubbles that collapse during the shedding when the pressure rises downstream again. The transition from steady to transient states is quite snappish, probably due to the short nozzle length in this case (nozzle ratio L_n/w_n<5), being this fact an added difficulty for the CFD modeling, Coussirat et al., 2016-2021a.

3. SETUP DEFINED FOR CFD SIMULATIONS

A commercial CFD code, Ansys, 2020, was used for the simulations. A two-dimensional (2D) structured mesh was defined (50,000 hexahedral cells, cell length h=0.04mm=4.0×10^{-5}m=40μm), Fig.1. A grid sensitivity study and a comparison between 2D and 3D (~2.5×10^6cells) meshes ensure both grid independence for this mesh (M03) and negligible differences in the predicted 2D/3D flow fields, Coussirat et al., 2021. The following boundary conditions were defined for each σ case, Fig.1: 1)Inlet, a mean velocity computed from the flow rate. 2)Outlet, a p_{out} =1.0×10^5 Pa. 3)Walls, non-slip condition. 4)Turbulence levels at inlet/outlet, computed from standard formulations for k and ω. The discretization schemes used were: 1) Transient formulation, Bounded Second Order Implicit. 2) Spatial discretization for ρ, k, ω and *vf,* QUICK. 3)Gradients, Least Squares Cell based. 4)Momentum, Bounded Central Differencing; pressure SST/SAS, PRESTO/Body Force Weighted. 3) Pressure-velocity coupling SST/SAS: SIMPLEC/PISO, see full details in Versteeg et al., 2007, Ansys 2020. The time-step was estimated, using the typical integral (production) and Kolmogorov (dissipation) scales, Tennekes et al., 1972, Thing 2016, and compared against ones computed by the Courant criteria, Table.1. The integral scales based in l were computed by means of the turbulent Reynolds number, Re_τ, Eq.6,

$$\mathrm{Re}_\tau = \frac{u^* l}{\nu};\ \mathrm{Re}_L = \frac{c_{m,out} L_n}{\nu};\ u^* = c_{m,out}\left(\frac{c_f}{2}\right)^{1/2}, c_f = 0.058(Re_L)^{-1/5};\ \mathrm{Re}_\eta = \frac{u_\eta \eta}{\nu} \sim 1$$
$$\delta = 0.38 L_n (\mathrm{Re}_L)^{-1/5};\ l/\eta = (\mathrm{Re}_\tau)^{3/4};\ u_l/u_\eta = (\mathrm{Re}_\tau)^{1/4};\ t_l/t_\eta = (\mathrm{Re}_\tau)^{1/2}. \quad (6)$$

Being: u^* the friction velocity, l=$f(\delta)$ the size of the large (energetic) eddies, η the size of the small (dissipative) eddies, δ the boundary layer thickness and t_l, t_η the energetic and dissipative time scales respectively. Because it is assumed that there is not a developed flow into the nozzle, White 2011, the friction coefficient c_f is computed using flat plates formulations, Schlichting 2000. The

energetic (integral) scale, the Kolmogorov eddies length scale and the energetic/dissipative time scales, (t_l., t_η) computed can be seen in Table.1.

Table.1: Values computed from definitions in Eq.6. T_c is the time-step computed using the Courant number definition, Co=$T_c\, c_{nozzle}/h$. The dissipation rate, ε [m^2/s^3] is a function of c_{nozzle} and $l=\delta$ at L_n, Thing 2016.

σ	c_{nozzle} [m/s]	Re	Re_L	c_f	u^* (m/s)	δ [m] at L_n	Re_τ	T_c [s]	$\varepsilon = c_{nozzle}{}^3/l$	η [m]	t_η [s]	u_η [m/s]	Re_η	l [m]	t_l [s]
1.19	12.83	27700	99148	5.81E-03	0.69	3.05E-04	219	1.56E-06	6.94E+07	3.56E-07	1.22E-07	2.91	1	3.05E-05	5.07E-04
0.94	14.44	31200	111556	5.67E-03	0.77	2.97E-04	238	1.39E-06	1.01E+08	3.24E-07	1.01E-07	3.20	1	2.97E-05	4.51E-04
0.82	15.46	33500	119440	5.60E-03	0.82	2.93E-04	250	1.29E-06	1.26E+08	3.06E-07	9.07E-08	3.38	1	2.93E-05	4.20E-04

The T_c estimation from the Courant number gives values $t_l<T_c<t_\eta$. Then, the defined grid size (h=4×10^{-6}m) and the computed time-step, T_c, allow to calculate the energetic eddies behavior during the simulations. The space- and time- scales already defined, guarantee the suitable cutting between the modeled and the computed eddies, in concordance with the 'classical EVMs' capabilities related to the 'turbulent cascade' modeling concept, Tennekes et al., 1972, Thing 2016. Taking these scales into account also makes it possible to avoid the phenomenon of aliasing in the predicted shedding frequencies, f_{vs}. Finally, 60 iterations by time-step were sufficient to obtain convergence in each time-step using the Bounded Second Order Implicit scheme, Ansys 2020.

4. CFD SIMULATIONS OF SLIGHT/FULL DEVELOPED CAVITATION STATES

A set of URAS/EVM CFD were carried out for σ=1.19 and σ=0.94, using the calibrated (by $\beta^*{}_\infty$ and C_s) SST and SAS-SST models. In each case, a precursor simulation to obtain an initial condition for the vortex shedding was performed, accounting for a fluid particle residence time into the nozzle of O(10^{-4}s). Then, the time defined for this simulation was 5 times bigger than the residence time and a total time of O(10^{-3}s), necessary to compute 4-6 cavity evolution cycles, was simulated. The obtained results from URAS/EVM simulations for each case computed (*CPU Intel/CoreTM2, CuadQ9400/266GHz, 16GB, 45 s/time-step, i.e.,~72hs/CPU for precursor and ~72hs/CPU for shedding*) was compared against the experiments and the CFD results obtained by LES (*Linux computer, 3.0GHz×32cores, 16 CPU and 64GB memories/node, time-steps of 10^{-8}s, about 700,000 cells, h=4μm, a three-weeks/CPU for a precursor CFD to define the inlet boundary condition and one-week/CPU to compute the shedding using 2,800,000 cells in the nozzle simulations*) see full details in Sou et al., 2014 and Biçer 2015.

In the σ=1.19 case, results obtained for the *vf* levels by means of the calibration tasks, showed low *vf* level predictions and slight variations of these levels for SAS-SST models (0.09<$\beta^*{}_\infty$<0.18 and 0.11<C_s<0.20 ranges, not shown). On the other hand, the SST results give higher *vf* levels confirming the previous results obtained by Coussirat et al., 2021a,b. Otherwise, the calibration tasks for the σ=0.94 case allow to see the improvements in the $\nu_{t,m}$ predictions obtained by the SAS-SST model compared against the SST model (i.e., higher *vf* levels and a more accurate cavity shape estimations were obtained) see Fig.2 and Fig.3 respectively. The obtained results using a calibrated SAS_SST model showed similar quality as LES ones but avoiding intensive CPU requirements. More in detail, it was observed that higher *vf* values and a slightly better cavity breaking/shedding are predicted for the SAS_SST model when C_s =0.2, whereas the SST model underpredicts the *vf* level, despite that a vortex shedding is observed too. Surprisingly, uncalibrated SAS-SST ($\beta^*{}_\infty$=0.09, C_s=0.11) gives *vf* values nearest to 1.0 but the shedding is mitigated leading to a 'steady' cavity (this simulation was stopped at t=9.5e-4s, see Fig.3). Notice that a *vf* level of O(~1) was assumed for the visualised experimental cavity, remarking that an exact *vf* level comparison against CFD results could not be carried out.

Concerning the shedding, i.e, f_{vs}, these frequencies were estimated for σ=1.19 and σ=0.94 cases obtaining the time series signal for the *vf* evolution in the P04 and P10 stations (Fig.3 shows the

σ=0.94 case). A Fast Fourier Transform (FFT) was applied to these time signals and the *vf* Power Spectral Density (PSD) at positions P04 and P10 and its characteristic frequencies were computed, see Table.2 and Fig.4.

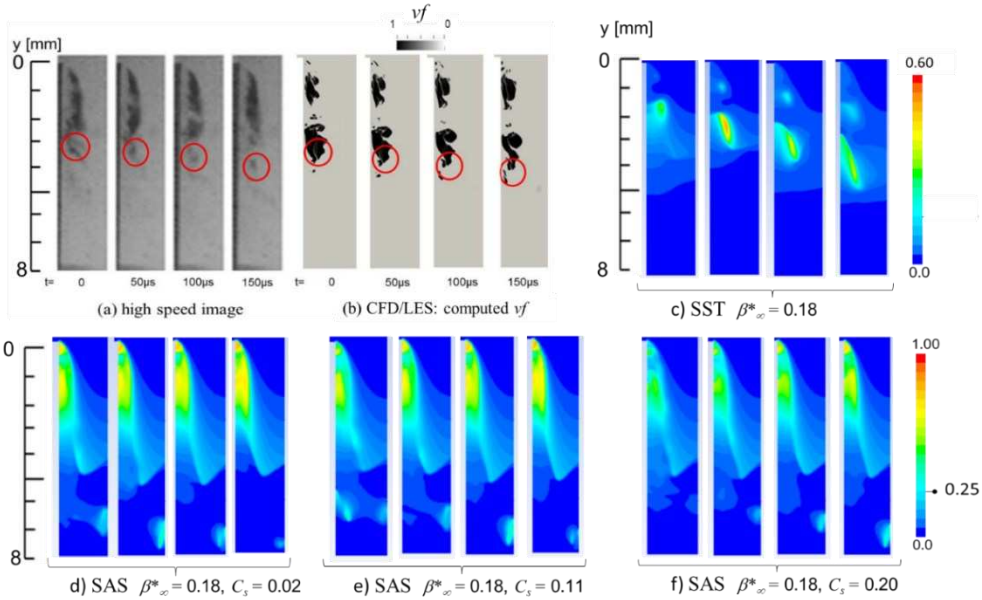

Fig.2: Cavity shape and *vf* evolution into the shedding cycle (σ = 0.94). (a)Experiments, high speed images; (b) CFD/LES modeling (Sou et al., 2014, Biçer 2015). **(c-f)** Present CFD results for calibrated SST and SAS-SST models. Notation: *t* = time-step, *vf* = vapor fraction. Notice the different *vf* scales for SST and SAS-SST.

.

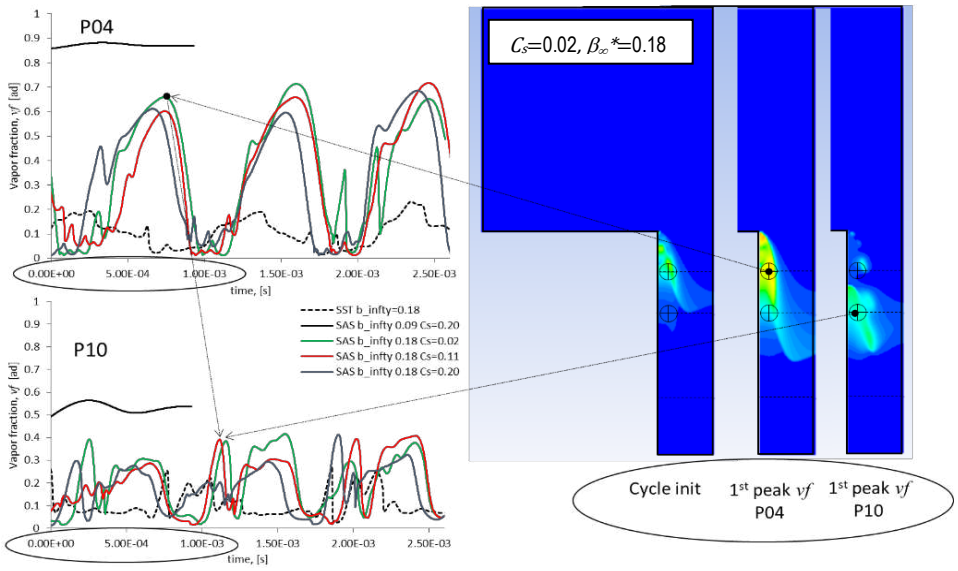

Fig.3: σ=0.94: *vf* evolution for the shedding cycle. Notation: β^*_∞=b_infty. *vf* scale: idem as SAS-SST, Fig.2.

The obtained f_{vs} results by SAS-SST were almost insensitivity to the C_s coefficient tunning in the σ=0.94 case, , see Fig.4, despite that more frequencies are observed when the C_s value goes down allowing the model to operate in LES mode, providing a strong enough flow instability to generate more turbulent structures in the separated zone. More C_s sensitivity is observed at σ=1.19 due to the higher f_{vs} values predicted, like experiments shows, Gavaises et al., 2015.

Table.2: Computed values for f_{vs} 1st mode and comparisons against results from Trummler et al., 2020, (CFD) and experiments from Gavaises et al. 2015 (Re=31,000, σ=0.92) and Zixhia et al., 2016 (Re=13,500, σ = 1.008).

Exp.- CFD/Turbulence model	σ	*Range of* f_{sv} [kHz]
Exp., Zixhia et al., 2016	1.008	2.8
Exp., Gavaises et al., 2015	0.92	1.0 – 2.0
CFD/LES, Trummler et al., 2020	1.19 / 0.82	1.11 – 0.75
CFD/SST (P04,P10)	1.19 / 0.94	1.17 – 0.87 / 1.17 – 0.87
CFD/SAS-SST (P04,P10)	1.19 / 0.94	0.85 –1.10 / 1.28 – 1.10

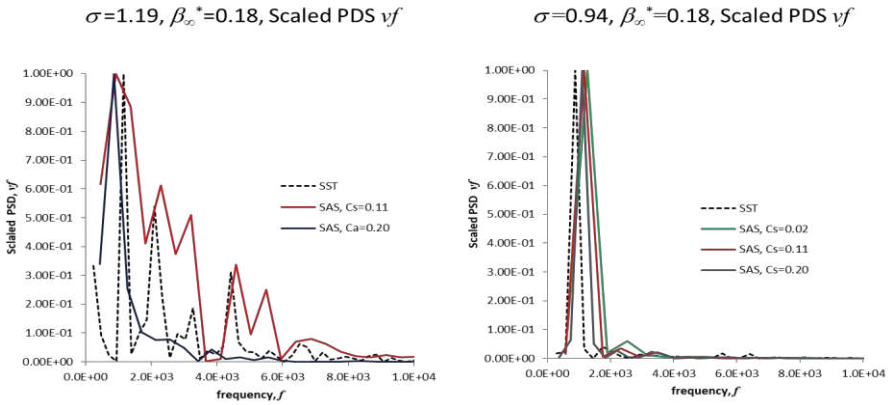

Fig.4. Shedding frequencies at P04 position. Notation: PSD *vf* Power Spectral Density vapor fraction.

5. CONCLUSIONS

A numerical study of developed cavitating flow in asymmetrical injector nozzle by means of URAS/EVM simulations were carried out using calibrated SST and SAS-SST models. Both the cavity shape and the vortex shedding frequencies (f_{vs}) were obtained by these two models for slightly developed cavitation (σ=1.19) and fully developed cavitation (σ=0.94) case. The *vf* was underestimated by the calibrated SAS-SST model for σ=1.19, but it gives *vf* levels nearer to the experimental ones in the σ=0.94 case. Concerning to the cavity shedding, the f_{vs} 1st mode predicted by the SAS-SST model is like ones reported in experiments and in CFD/LES simulations by several authors for similar σ and Re numbers. Also, the evolution of the cavity shape predicted shows some similarities with the experimental data from Sou and Biçer. The SAS-SST model shows a more complex cavity shape and more shedding frequencies than the SST model in both cases. The SST model and the SAS-SST (at P10) captures the same trend as experiments show for the $f_{vs}=f(\sigma)$, i.e., a rising in the f_{vs} when σ rises. On the contrary the SAS-SST model does not show this trend at (P04). These results allow concluding that there is a clear relation between the $\nu_{t,m}$ predicted, and the subsequent pressure field computed, leading to a rising in the *vf* level predicted and more complex cavity shape including vortex shedding. The obtained results are competitive compared to those obtained by LES in terms of CPU time saving, then the SAS functionality could be more explored to open the possibility to perform URAS/EVM CFD with affordable CPU costs in 3D cases with complex geometry. As a future work it is pointed out that more SAS-SST calibration tasks are necessary to obtain better f_{vs} fitting to recover the $f_{vs}=f(\sigma)$ trend that experiments show.

ACKNOWLEDGEMENTS

This current work was partially supported by the Universidad Tecnológica Nacional (UTN) within its own research programme (UTN/SCTyP). Authors would like to express their appreciation to the UTN for providing financial support for this study (research project AMTCAME0008441TC).

REFERENCES

Ansys/Fluent Software, 2020, http://www.ansys.com/Industries/Academic/Tools/ v15Tutorial.
Biçer B., Cavitation Phenom. inside Fuel Injector Nozzles, *PhD Thesis*, *Kobe Univ.* Japan, 2015.
Coussirat, M., Moll, F., Cappa, F., and Fontanals A., Study of Available Turbulence and Cavitation Models to Reproduce Flow Patterns in Confined Flows,", *J. Fluids Eng*., 138(9), 2016.
Coussirat M., Moll F. and Fontanals A., Reproduction of the cavitating flows patterns in several nozzle geom. using calibrated turb. and cavitat models, *Mec.Comput.,*35, 2017.
Coussirat, M., Moll, F., Recalibration of EVMs for Numerical Simulation of Cavitating Flow Patterns in Low Pressure Nozzle Injectors. *J. of Fluids Engineering*, 143(3), 031503, 2021.
Coussirat, M., Moll, F., CFD of Cavitating Flow in Asymmetrical Nozzles of Injectors. Part I. Assessment of Calibrated EVMs in Developing Cavitation Cases. Part II. Application to Fully Developed Cavitation Cases. *Mec. Computac.*, 38, 2021.
De Giorgi, M. G., Ficarella A., and Tarantino M., Evaluating cavitation regimes in an internal orifice at different temperat. using freq. analysis and visualizat. *Int.J. Heat Fluid Flow* 39, 2013.
Egorov and Menter, Develop. and Applicat of SST-SAS Turb. Model in the DESIDER Project, Adv. in Hybrid RANS-LES Modelling, NNFM 97, Springer, 2008.
Egorov, Y., Menter, F., Lechner, R., and Cokljat, D., The SAS Method for Unsteady Turbul. Flow Predictions, Part 2: Application to Complex Flows, *Flow Turb. Comb*., 85(1), pp.139–165, 2010.
Gavaises M, Villa F., Koukouvinis P., Marengo M., Franc J, Visualiz. and LES simulat. of cavitation cloud formation and collapse in an axisymm geom., Int.J Multiph. Flow 68(14), 2015.
Korkut E. and Atlar M., On the importance of the effect of turbulence in cavitation inception tests of marine propellers, *Proc. R. Soc. Lond. A*, 458, pp29-48, 2002.
Menter F., 'Two Equation Eddy-Viscosity Turb. Models for Eng. Appl.,', *AIAA J.*, 32(8),1994.
Menter F and Egorov Y., A scale adaptive simulation model using two-equation models. In 43rd AIAA aerospace sciences meeting and exhibit (p. 1095), 2005.
Menter, F., and Egorov, Y., 'The SASimulation Method for Unsteady Turbul. Flow Predictions—Part 1: Theory and Model Description,' *Flow Turb. Comb.*, 85(1), 2010.
Mitroglou N., Stamboliyski V., Karathanassis K., Nikas K., Gavaises M., Cloud cavitation vortex shedding inside an injector nozzle, *Exp. Thermal and Fluid Science*, 2017
Schlichting, H., Gersten, K., *Boundary Layer Theory*, 8th ed. Springer, Berlin, 2000.
Shi J. and Arafin M., CFD investigation of fuel property effect on cavitating flow in generic nozzle geometr., *ILASS–Eur2010, 23rd Ann. Conf. on Liquid Atomiz. and Spray Syst.*, Czech Rep., 2010.
Sou A., Biçer B., Tomiyama A., Num. simulation of incipient cavitating flow in a nozzle of fuel injector, *Comp&Fluids* 103, 2014.
Singhal, A., Athavale, M., Li, H., and Jiang, Y., Math. Basis and Validation of Full Cavitation Model, *J. Fluids Eng.* 124(3), 2002.
Stanley, C., Barber, T. and Rosengarten, G., Re-Entrant Jet Mechanism for Periodic Cavitation Shedding in a Cylindrical Orifice. *Int J. Heat and Fluid Flow*, 50, 2014.
Trummler T., Schmidt, S., Adams N., Investigation of condensation shocks and re-entrant jet dynamics in a cavitating nozzle flow by LES, *Int. J. Multiphase Flow*, 125, 2020.
Versteeg H. and Malalasekera W., 2007, *An Introduction to Computational Fluid Dynamics: The Finite Volume Method*, 2nd Ed., Upper Saddle River, NJ, USA, Pearson Prentice Hall; 2007.
Thing D., *Basics of Engineering Turbulence*, Academic Press, Elsevier, 2016.
Tennekes, H., Lumley, J., *A first course in turbulence*, MIT press., 1972.
Wang Z., Zhang M., Kong D., Huang B., Wang G., Wang C., The influence of ventilated cavitation on vortex shedding behind a bluff body, *Exp. Therm Fluid Sci.*, 98, 2018.
White F., *Fluid Mechanics*, 7th ed. McGraw Hill, New York. 2011.
Zhixia H., Yuhang C., Xianyin L., Qian W., Genmiao G., Exp. Visualiz. and LES investig. on cloud cavitation shedding in rectangular nozzle orifice., *Int. Comm. Heat Mass Transfer* 76, 2016.